Simplify Modeling and Implement of A Hybrid Resonant Converter Operating in DCM and CCM with State Feedback Control

Rong-Tai Chen, and Yung-Yaw Chen

Department of Electrical Engineering, National Taiwan University, Taipei, Taiwan , R. O. C
E-mail (first): rtchen@ipmc.ee.ntu.edu.tw, E-mail (second): yychen@ntu.edu.tw

Abstract—**A state plane approach to the steady state analysis and design of the high-order hybrid resonant converter operated in the CCM and DCM is presented. The sampled-data approximated dynamic model is also obtained. A state feedback control technique that can be easily implemented is proposed to improve the stability and dynamic characteristic of resonant converters. A prototype unit has been built to verify the theoretical results. The experimental results confirm the validity of the proposed control.**

I. INTRODUCTION

Resonant converters have many advantages over the conventional pulsewidth modulation (PWM) converters such as low switching losses at higher switching frequencies, easier electromagnetic interference (EMI) filtering, smaller size and weight of components, etc.[1]-[7]. On the other hand, the presence of a high-frequency resonant tank circuit makes resonant converter operation more complex and control more difficult than PWM converters [3][6].

The proposed hybrid resonant converter will work in continuous conduction mode (CCM) or discontinuous conduction mode (DCM). When the switching frequency (ft) larger half of the resonant frequency (fo), that is ft > 1/2 fo , it works in CCM; otherwise it works in DCM, that is ft < 1/2 fo. Some results on the DC characteristic curves were reported in [1]-[8], assuming sinusoidal excitation. The analysis given in [2][9] is based on the time-domain state space approach in which the solution procedure is rather complex. On the other hand, in [4][7], using the state-plane diagram technique, but they never consider converter operating in DCM. In this paper, based on the steady-state response derived, we present a complete closed-form analysis for the hybrid resonant converter operated in CCM and DCM.

A simple nonlinear discrete-time dynamic model for the proposed converter is derived using approximations to most power converters[6][10]. In the proposed model the tank states are treated as discrete quantities and the filter states are treated as continuous time averaged states. The tank element circuit model consists in general of discrete energy states, but may be approximated by a low frequency continuous time model. These equivalent circuit models completely characterize the terminal behavior of the converters, and are solvable for any transfer function or impedance of interest. Closed form solutions are given for the equivalent circuit models of the converter.

Resonant converters have two sets of energy storage elements. One is the output filter with a slow time constant, and another is the resonant circuit with a fast time constant. In the past, designers have used the slow output filter information to control the switching frequency [5], [11]. Such a controller has a limitation on the control of the fast resonant circuit because of the slow output filter information. In this paper, a state feedback control technique that can be easily implemented is proposed to improve the stability and dynamic characteristics of resonant converters. Closed form expressions for the small signal models of proposed converters are obtained. The performance of the hybrid resonant converter and the effectiveness of the proposed design approach are demonstrated by some experiment results.

II. STEADY STATE ANALYSIS

Fig. 1 shows a schematic diagram of a hybrid resonant converter system. To simplify the analysis, we assume that the switch devices D1/T1 and D2/T2 are ideal. Thus, we may represent the equivalent source vg(t) with amplitudes equal to ± E. Furthermore, the load current Io is considered constant since a large filtering inductance Lo is assumed at the output circuit. Consequently, the current input to the bridge rectifier $i_D(t)$ has constant amplitudes +Io and – Io, depending on whether the voltage Vcp(t) is positive or negative, respectively.

A set of typical steady state voltage and current waveforms for the hybrid resonant converter operated in CCM and DCM are shown in Fig. 2.

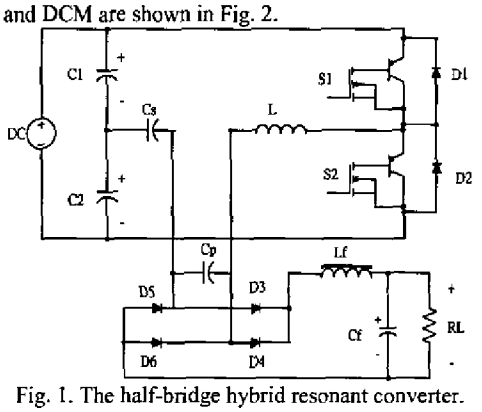

Fig. 1. The half-bridge hybrid resonant converter.

0-7803-8730-9/04/$20.00 ©2004 IEEE

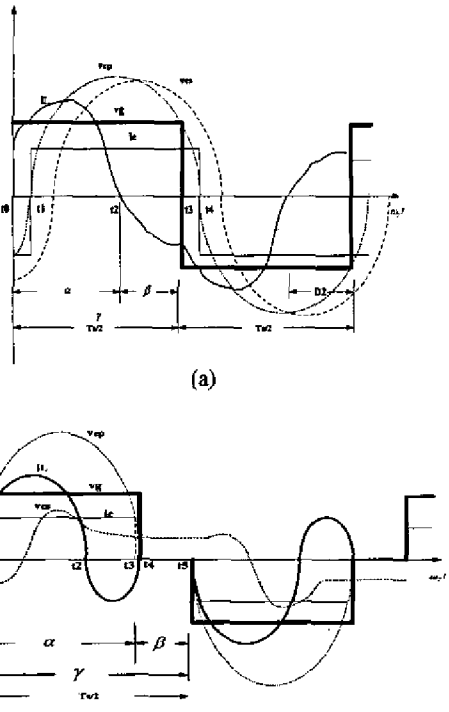

(a)

(b)

Fig. 2. Typical waveforms of the proposed converter operated in (a) CCM (b) DCM.

A. Steady state trajectory

The steady state response of the converter can be derived from the proposed circuit of Fig. 1. It represents a third order nonlinear system, which are difficult to solve by the conventional time domain approach. However, it can be shown that by proper transformation on its state variables, the steady state solution can be derived from a two-dimensional state plane analysis. Let us define a new state variable Vc(t) as shown in eq. (1).

$$V_c(t) = V_{cp}(t) + V_{cs}(t) \tag{1}$$

Using this transformation, the mathematical description for the circuit model of Fig. 1 can be simplified to the following.

$$\frac{d\,i_L(t)}{dt} = \frac{1}{L}V_g(t) - \frac{1}{L}V_c(t) \tag{2}$$

$$\frac{d\,V_c(t)}{dt} = (\frac{1}{C_s} + \frac{1}{C_p})\,i_L(t) - \frac{1}{C_p}\,i_D(t) \tag{3}$$

If we normalized the currents and voltages in eq.(2) and (3) by E/Zo and E, respectively, then in terms of the state-plane equation form, it can be written as follows,

$$\frac{d\,V_{cn}(t)}{d\,i_{Ln}(t)} = \frac{i_{Ln}(t) - i'_{Dn}(t)}{V_{csn}(t) - V_{cn}(t)} \tag{4}$$

where $i_{Dn}'(t) = \left[1 - (\frac{\omega_{OS}}{\omega_O})^2\right] i_{Dn}(t)$, $\omega_O = \frac{1}{\sqrt{L\,C_T}}$,

$\omega_{OS} = \frac{1}{\sqrt{L\,C_S}}$, $\frac{1}{C_T} = \frac{1}{C_S} + \frac{1}{C_p}$, $Z_o = \sqrt{\frac{L}{C_T}}$

Eq. (4) can be solved by a piece-wise linear analysis over the time intervals where i'_{Dn} and V_{csn} are constants[1].

Case I : CCM

Over a switching period Ts, it can be shown that there exist four time intervals where the solution of eq. (4) consists of four circular arcs in the V_{cn} - i_{Ln} plane. The radii Rin can be expressed in terms of the boundary voltages and currents, i.e.

$R_{in}^2 = (V_{cn}(t_O) \pm 1)^2 + (i_{Ln}(t_O) \pm I_{on}')^2$ i=1,2,3,4 , where

$R_{1n}=R_{3n}$, $R_{2n}=R_{4n}$ and $I_{on}' = \left[1 - (\frac{\omega_{OS}}{\omega_O})^2\right] I_{on}$.

Case II : DCM

Over a switching period Ts, it can be shown that there exist six time intervals where the solution of eq. (4) consists of six circular arcs in the V_{cn} - i_{Ln} plane. The radii Rin can be expressed in terms of the boundary voltages and currents, i.e.,

$R_{in}^2 = (V_{cn}(t_O) \pm 1)^2 + (i_{Ln}(t_O) \pm I_{on}')^2$ $i = 1,2,...,6$ where

$R_{1n}=R_{3n}=R_{4n}=R_{6n}$ and $R_{2n}=R_{5n}$.

Under CCM and DCM steady state conditions, the typical state plane diagrams for the proposed converter over a switching period are shown in Fig. 3 (a) (b), respectively. The portions of the trajectory shown by solid and broken lines represent the response over the half switching periods for Vcsn=1 and Vcsn=-1, respectively.

B. Steady state characteristics

The converter DC output voltage can be calculated from,

$$Vo = \frac{2}{T_s}\int_0^{0+\frac{T_s}{2}} |V_{cp}(t)|\,dt \tag{5}$$

where the absolute magnitude sign is used due to the presence of the full bridge rectifier at the output circuit.

It can be shown that by using eqs. (2) and (3) and with some mathematical manipulations, evaluation of the integral in eq. (5) will derive the converter gain to following expression,

$$M = \frac{V_o}{V_g} = \frac{1}{\gamma}\left[1 - (\frac{\omega_{OS}}{\omega_O})^2\right]\left[(\gamma - 2\beta 1) + 2\,i_{Ln}(t_1)\right] \text{ for CCM} \tag{6}$$

$$M = \frac{V_o}{V_g} = \frac{\beta}{\gamma}\left[1 - (\frac{\omega_{OS}}{\omega_O})^2\right] \text{ for DCM} \tag{7}$$

From the geometric properties of the state plane diagram given in Fig. 3, it can be shown that the following relation must hold

$$i_{Ln}(t_1) = -\frac{V_{cn}(t_0)}{I'_{on}} \tag{8}$$

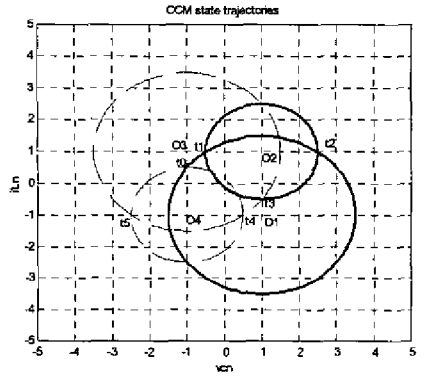

(a)

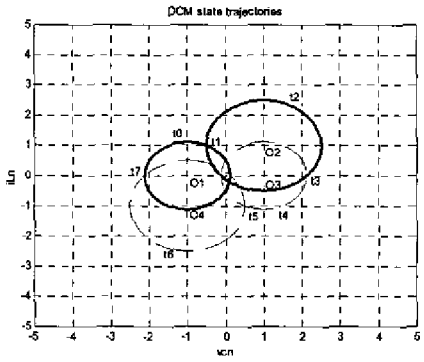

(b)

Fig. 3. Typical steady state trajectory in (a) CCM (b)DCM.

Substituting eq. (8) into eq. (6), the gain M becomes,

$$M=\frac{V_o}{V_g}=\frac{1}{\gamma}\left[1-\left(\frac{\omega_{os}}{\omega_o}\right)^2\right]\left[(\gamma-2\beta 1)-\frac{2V_{on}(t0)}{I_{on}'}\right] \quad (9)$$

where $\beta_1=\omega_o(t_1-t_0)$, $\gamma=\omega_o\cdot\frac{T_s}{2}$ and α is the conduction angle of D1, β is the conduction angle of T1.

Given operating mode, the converter gain M, the average diode current are plot in Fig. 4.(a) (b), respectively, as a function of switching frequency.

It can be shown that under the same loading conditions, the peak capacitor voltage across cp and the peak inductor current are lower than their counterparts in the conventional PRC.

III. DYNAMIC MODELING OF THE PROPOSED CONVERTER

Due to the symmetrical operation of a resonant converter over a complete switching interval, the discrete time domain description needs only to be carried out over half the switching interval, Ts/2. If we consider only small perturbations of the states, inputs, and outputs superimposed on the corresponding operating point values then the state equations can be linearized. The result will be useful for modeling the small signal frequency response of systems whose loop bandwidth is much less than one-half the sampling frequency. Consequently, we can derived the dynamic equations of the proposed converter as follows from the previous process.

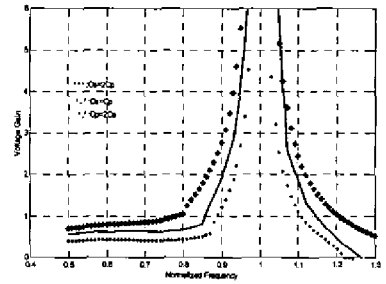

(a)

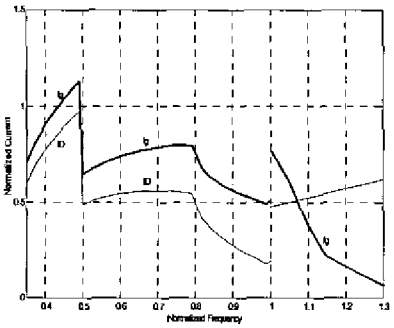

(b)

Fig. 4. Characteristics curves for the proposed converter (a) voltage gain (b) the average input and diode current

Case I CCM

$$\begin{bmatrix}\dot{\hat{x}}_1\\ \dot{\hat{x}}_2\end{bmatrix}=\begin{bmatrix}a_{11} & a_{12}\\ a_{21} & a_{22}\end{bmatrix}\begin{bmatrix}\hat{x}_1\\ \hat{x}_2\end{bmatrix}+\begin{bmatrix}b_{11} & b_{12}\\ b_{21} & b_{22}\end{bmatrix}\begin{bmatrix}\hat{I}_o\\ \hat{\beta}\end{bmatrix}$$

$$\hat{v}_o=\begin{bmatrix}c_1 & c_2\end{bmatrix}\begin{bmatrix}\hat{x}_1\\ \hat{x}_2\end{bmatrix}+\begin{bmatrix}d_1 & d_2\end{bmatrix}\begin{bmatrix}\hat{I}_o\\ \hat{\beta}\end{bmatrix} \quad (10)$$

where

$$a_{11}=\frac{\omega_o}{\gamma}\left[\cos(\alpha-\beta)-1\right]$$

$$a_{12}=\frac{\omega_o}{\gamma Z_o}\sin(\alpha+\beta)$$

$$a_{21}=\frac{\omega_o Z_o}{\gamma}\sin(\alpha+\beta)$$

$$a_{22}=\frac{\omega_o}{\gamma}\left[\cos(\alpha-\beta)-1\right]$$

$$b_{11}=\frac{\omega_o}{\gamma}(\frac{C_T}{C_P})[1-2\cos\beta+\cos(\alpha-\beta)]$$

$$b_{12}=\frac{\omega_o}{\gamma}\left[\begin{array}{l} i_{L(0)}\sin(\alpha-\beta)+\dfrac{V_g+v_{c(0)}}{Z_o}\cos(\alpha+\beta) \\ +(\dfrac{C_T}{C_P})I_o(2\sin\beta+\sin(\alpha-\beta)) \end{array}\right]$$

$$b_{21}=\frac{\omega_o}{\gamma}(\frac{C_T}{C_P})Z_o[\sin(\alpha+\beta)-2\sin\beta]$$

$$b_{22}=\frac{\omega_o}{\gamma}\left[\begin{array}{l} i_{L(0)}Z_o\cos(\alpha+\beta)+(V_g+v_{c(0)})\sin(\alpha-\beta) \\ +(\dfrac{C_T}{C_P})I_oZ_o(\cos(\alpha+\beta)-2\cos\beta) \end{array}\right]$$

$$c_1=\frac{2}{\gamma}(\frac{C_S}{C_S+C_P})Z_o\cos\alpha$$

$$c_2=\frac{2}{\gamma}(\frac{C_S}{C_S+C_P})\sin\alpha$$

$$d_1=\frac{1}{\gamma}(\frac{C_S}{C_S+C_P})(\frac{2C_T}{C_P}Z_o)(\cos\alpha-1)$$

$$d_2=\frac{1}{\gamma}(\frac{C_S}{C_S+C_P})\left[\begin{array}{l} (1-\gamma-2\sin\alpha)V_g-2v_{c(0)}\sin\alpha \\ -(\cos\alpha-1)(\dfrac{2C_T}{C_P}Z_o)I_o+2Z_oi_{L(0)}\cos\alpha \end{array}\right]$$

Case II DCM

$$\begin{bmatrix}\dot{\hat{x}}_1\\ \dot{\hat{x}}_2\end{bmatrix}=\begin{bmatrix}0 & 0\\ 0 & a_{22}\end{bmatrix}\begin{bmatrix}\hat{x}_1\\ \hat{x}_2\end{bmatrix}+\begin{bmatrix}0 & 0\\ b_{21} & b_{22}\end{bmatrix}\begin{bmatrix}\hat{I}_o\\ \hat{\beta}\end{bmatrix}$$

$$\hat{v}_o=\begin{bmatrix}0 & 0\end{bmatrix}\begin{bmatrix}\hat{x}_1\\ \hat{x}_2\end{bmatrix}+\begin{bmatrix}0 & d_2\end{bmatrix}\begin{bmatrix}\hat{I}_o\\ \hat{\beta}\end{bmatrix} \qquad (11)$$

where

$$a_{22}=\frac{\omega_o}{\gamma}\cos(\alpha-\beta)$$

$$b_{21}=\frac{\omega_o}{\gamma}(\frac{C_T}{C_P})Z_o[\sin(\alpha+\beta)-2\sin\beta]$$

$$b_{22}=\frac{\omega_o}{\gamma}\left[\begin{array}{l} (V_g+v_{c(0)})\sin(\alpha-\beta) \\ +(\dfrac{C_T}{C_P})I_oZ_o(\cos(\alpha+\beta)-2\cos\beta) \end{array}\right]$$

$$d_2=-\frac{\alpha(\gamma+1)}{\gamma^2}(1-(\frac{\omega_{os}}{\omega_o})^2)V_g$$

IV. DESIGN OF PROPOSED CONVERTER SYSTEM

For achieving more accurate system dynamic stability, a state feedback control technique is proposed in Section IV-A. Fig. 5 shows the block diagram with state feedback controller for the hybrid resonant converter. In section IV-B, a closed-loop voltage feedback controller is discussed.

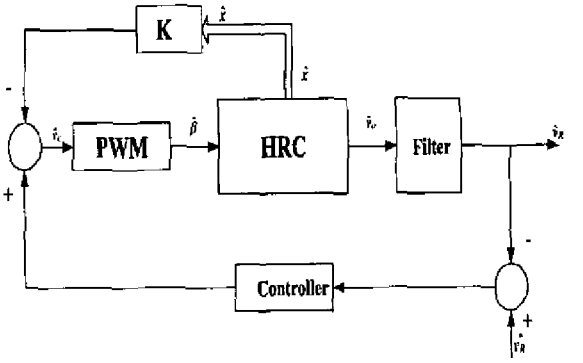

Fig. 5. The block diagram for the proposed system with state feedback controller.

A. Control law

Firstly, by ignoring the large time constant of the output filter and considering the dynamic effects of the resonant circuit, the proposed control law for the proposed converter operating above resonant frequency can be viewed on the two-dimensional state plane.

Since the control law determines the instant at which the Kth event is ended. It can be described as

$$k_1Z_o\hat{x}_1+k_2\hat{x}_2=v_c \qquad (12)$$

where vc is the control variable from voltage feedback.

From (10) and (12) , the linearized control law becomes

$$\hat{\beta}=-\frac{k_nZ_oa_{11}+a_{21}}{k_nZ_ob_{11}+b_{21}}\hat{x}_1-\frac{k_nZ_oa_{12}+a_{22}}{k_nZ_ob_{11}+b_{21}}\hat{x}_2\equiv-p\hat{x}_1-q\hat{x}_2$$

(for CCM) (13)

$$\hat{\beta}=-\frac{Z_oa_{11}+k'_na_{21}}{Z_ob_{11}+k'_nb_{21}}\hat{x}_1-\frac{Z_oa_{12}+k'_na_{22}}{Z_ob_{11}+k'_nb_{21}}\hat{x}_2\equiv-r\hat{x}_1-s\hat{x}_2$$

(for DCM) (14)

where $k_n=\dfrac{k_1}{k_2}$, $k'_n=\dfrac{k_2}{k_1}$

Substituting eq. (13), (14) into eq. (10) yields the equations governing the dynamics of controlled system as

$$\begin{bmatrix}\dot{\hat{x}}_1\\ \dot{\hat{x}}_2\end{bmatrix}=\begin{bmatrix}a_{11}-pb_{11} & a_{12}-qb_{11}\\ a_{21}-pb_{21} & a_{22}-qb_{21}\end{bmatrix}\begin{bmatrix}\hat{x}_1\\ \hat{x}_2\end{bmatrix} \text{ for CCM} \qquad (15)$$

$$\begin{bmatrix}\dot{\hat{x}}_1\\ \dot{\hat{x}}_2\end{bmatrix}=\begin{bmatrix}a_{11}-rb_{11} & a_{12}-sb_{11}\\ a_{21}-rb_{21} & a_{22}-sb_{21}\end{bmatrix}\begin{bmatrix}\hat{x}_1\\ \hat{x}_2\end{bmatrix} \text{ for DCM} \qquad (16)$$

The characteristic equation of the closed-loop system is

$$\lambda^2+\left[\frac{(a_{21}b_{11}-a_{11}b_{21})+k_nZ_o(a_{12}b_{21}-a_{22}b_{11})}{k_nZ_ob_{11}+b_{21}}\right]\lambda=0 \quad \text{(for CCM)} \qquad (17)$$

$$\lambda^2+\left[\frac{k'_n(a_{21}b_{11}-a_{11}b_{21})+Z_o(a_{12}b_{21}-a_{22}b_{11})}{Z_ob_{11}+k'_nb_{21}}\right]\lambda=0 \quad \text{(for DCM)} \qquad (18)$$

The reduction of order is indicated by the zero eigenvalue, and the dynamics of the controlled system developed only on the choice of kn or k'_n. The stability range of kn or k'_n can be found from $\lambda < 0$. In the proposed converter, it can be calculated kn > -0.8954 or kn < -1.4122 and k'_n<1 or k'_n>2. For a given equilibrium state, the response of the proposed controlled system after a disturbance is overdamped when kn is less than the critical kn and is underdamped when kn is greater than the critical kn. These critical kn curves are found by claiming $\lambda = 0$.

B. Closed-loop voltage controller

Generally , complete elimination of the effect of input voltage variation under various operating conditions is impossible. Although the effect of state variation on the output voltage is much faster than that of load current and it is neglected in the design of closed loop feedback voltage controllers. Fig. 6. shows the closed-loop transfer function block diagram of the proposed controller system.

To characterize the module dynamic response systematically, a transfer function called control-to-output is defined as $g_1(s) \equiv \frac{\hat{v}_o}{\hat{\beta}}$, another output-impedance $g_2(s) \equiv \frac{\hat{v}_o}{\hat{i}_o}$. The controller Cv shown in Fig.6 is the PI controller, Cv(s)= $\frac{k_p s + k_I}{s}$. The closed-loop transfer function of $\hat{v}_R$ to $\hat{i}_O$ is derived from Fig.6 as

$$Zc(s) \equiv \frac{\hat{v}_R}{\hat{i}_O} \equiv s\left(\frac{\sigma 1}{s+\delta 1} + \frac{\sigma 2}{s+\delta 2}\right) \qquad (19)$$

For evaluating the regulating performance, the output voltage response due to unit-step load current change is found as

$$vo(t) = \sigma 1\, e^{-\delta 1 t} + \sigma 2\, e^{-\delta 2 t} \qquad (20)$$

Suppose that $\delta 1$ and $\delta 2$ are all positive real and $\delta 2 > \delta 1$, Using (9) , one can find the time at which the maximum dip of $v_R(t)$ occurred and the maximum dip to be

$$t_m = \frac{1}{\delta 2 - \delta 1} \ln\left(\frac{-\sigma 1 \delta 1}{\sigma 2 \delta 2}\right) \qquad (21)$$

and

$$v_m = \sigma 1\left(\frac{-\sigma 1 \delta 1}{\sigma 2 \delta 2}\right)\left(\frac{\delta 1}{\delta 2 - \delta 1}\right) + \sigma 2\left(\frac{-\sigma 1 \delta 1}{\sigma 2 \delta 2}\right)\left(\frac{\delta 2}{\delta 2 - \delta 1}\right) \qquad (22)$$

respectively. According to the above analysis, the parameters k_p and k_I of the voltage controller Cv can be find using (21) and (22). In the design process described above, the minimum value of v_m can be obtained by letting t_m=0, i.e. the maximum dip is forced to occur at t=0.

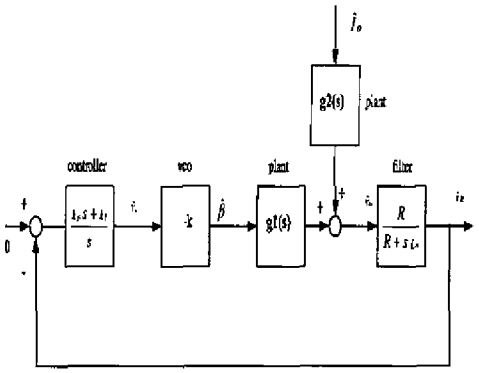

Fig. 6. Closed-loop transfer function block diagram of the proposed system.

V. EXPERIMENT RESULTS

In order to evaluate the validity of the theoretical results, the half-bridge hybrid resonant converter is implemented. This converter has the following parameters:
L=3.64 uH ; Cs=0.68 uF ; Cp=0.68 uF ;Vg= 48 V ; Io= 5 A, Inductor current waveforms, parallel and series capacitor waveforms with respect to CCM or DCM are shown in Fig. (7) –(9). To show the robustness of the controlled system with respect to the change in operating point, the step change of operating conditions are varied, as is shown in Fig. 10. It can be seen in this figure, the experiment shows that the dynamics of the system with this proposed control is insensitive to the variation of system operating point for considerable range. As is shown in Fig.10 the proposed control can provide much better dynamic response than the frequency control.

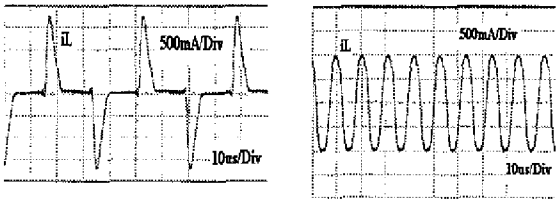

(a) (b)

Fig.7. Experiment results of inductor current (a) DCM (b) CCM.

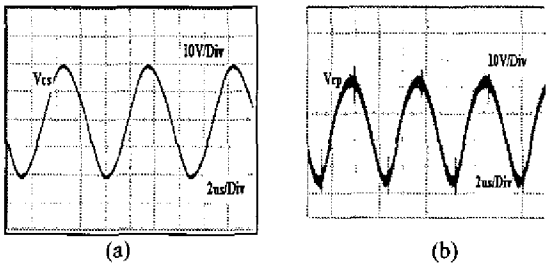

(a) (b)

Fig.8. Experiment results of CCM series and parallel voltage (a) Vcs (b) Vcp.

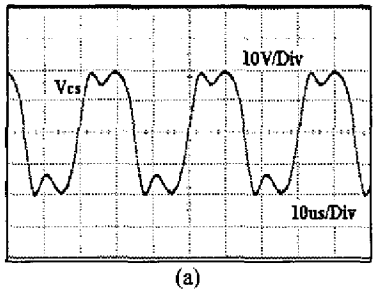

(a)

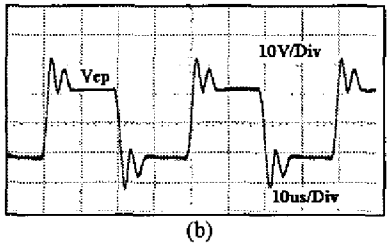

(b)

Fig.9. Experiment results of DCM series and parallel voltage (a) Vcs (b) Vcp.

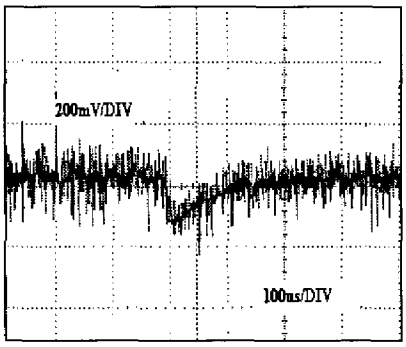

Fig.10. Experiment results of output voltage for step dynamic responses.

VI. CONCLUSIONS

This paper has presented a technique to calculate the steady-state solution for a hybrid resonant converter using state-plane trajectory techniques. A complete closed-form analysis operated in CCM and DCM is derived. A discrete dynamic model for a hybrid resonant converter was derived using approximations which most practical DC-DC converters meet. A general analytical procedure for the equivalent circuit modeling of resonant converters is presented. A state feedback control that can be easily implemented is proposed to improve the static and dynamic characteristics of resonant converters. The important characteristic of the system with this proposed control is the reduction of order due to the dependent nature of the state variables in the discrete time domain. The experimental results show good agreement with the theoretical analysis, and the excellent static and dynamic characteristic of the converter can be obtained by selecting the design parameter kn

VII. REFERENCES

[1] Issa Batarseh, C. Q. Lee, "Theoretical and Experimental Studies of the LCC-Type Parallel Resonant Converter," *IEEE Trans. Power Electron,* vol. 5, no. 2, pp. 140-150, April . 1990.

[2] R.J. King, T.A. Stuart, "A Large-Signal Dynamic Simulation for the Series Resonant Converter," *IEEE Trans. On Aerospace and Electronic Systems* , vol. AES-19, no. 6, pp. 859-870, November . 1983.

[3] Marn Go Kim, Dae Sik Lee, and Myang Joong Youn, "A new State Feedback Control of Resonant Converters ," *IEEE Trans. On Industrial Electronics,* vol. 38, no. 3, pp. 173-179, June . 1991.

[4] R.J. King, T.A. Stuart, "A Normalized Model for the Half-bridge Series Resonant Converter," *IEEE Trans. On Aerospace and Electronic Systems* , vol. AES-17, no. 6, pp. 190-198, March . 1981.

[5] R. Oruganti, J. J. Yang and F. C. Lee, "Implementation of Optimal Trajectory Control of Series Resonant Converter." IEEE Power Electron. Specialists Conf. Rec.. 1987, pp. 451-459.

[6] M. E. Elbuluk, G. C. Verghese, and J. G. Kassakian, "Sampled-data Modeling and Digital Control of Resonant Converter," *IEEE Trans. Power Electron,* vol. 3, pp. 344-354, July 1988.

[7] Ashoka K. S. Bhat, " A Unified Approach for the Steady-State Analysis of Resonant Converters ," *IEEE Trans. On Industrial Electronics,* vol. 38, no. 4, pp. 251-259, August . 1991.

[8] Tamotsu Ninomiya, Masatoshi Nakahara, and Koosuke Harada, "A Unified Analysis of Resonant Converters," *IEEE Trans. Power Electronics,* vol. 6, no. 2, pp. 260-270, April . 1991.

[9] Steven Morrison, "Analysis of a Hybrid Series Parallel Resonant Bridge Converter," *IEEE Trans. Power Electronics,* vol. 7, no. 1, pp. 119-127, January . 1992.

[10] Arthur F. Witulski, Ad'an F. Hernandez, and Robert W. Erickson, "Small Signal Equivalent Circuit Modeling of Resonant Converters," *IEEE Trans. On Power Electronics,* vol. 6, no. 1, pp. 11-27, January. 1991.

[11] Vijayakumar Belaguli, and Ashoka K. S. Bhat, "A Hybrid Resonant Converter Operated as a Low Harmonic Rectifier with and Without Active Control," *IEEE Trans. On Power Electronics,* vol. 14, no. 4, pp. 730-742, July. 1999.

[12] Vijayakumar Belaguli, and Ashoka K. S. Bhat, "Characteristics of Fixed-Frequency Hybrid Resonant Converter Operating on the Utility Line," *IEEE Trans. On Power Industry Applications,* vol. 35, no. 6, pp. 1413-1423, November/December. 1999.